Superfocussing in a metal-coated tetrahedral tip by dimensional reduction of surface-to edge-plasmon modes

K. Tanaka, G.W. Burr, T. Grosjean, T. Maletzky, U.C. Fischer

Superfocussing in a metal-coated tetrahedral tip by dimensional reduction of surface-to edge-plasmon modes

K. Tanaka · G.W. Burr · T. Grosjean · T. Maletzky · U.C. Fischer

Abstract Metal-coated dielectric tetrahedral tips (T-tip) have long been considered to be interesting structures for the confinement of light to nanoscopic dimensions, and in particular as probes for scanning near-field optical microscopy. Numerical investigations using the Finite-Difference Time-Domain (FDTD) method are used to explore the operation of a T-tip in extraction mode. A dipole source in close proximity to the apex excites the tip, revealing the field evolution in the tip, the resulting edge and face modes on the metal-coated surfaces, and the coupling from these modes into highly directional radiation into the dielectric interior of the tip. These results are the starting point for illumination-mode numerical investigations by a Volume Integral equation method, which compute the field distribution that develops in a T-tip when a Gaussian beam is incident into the tip, and which show that a highly confined electric field is produced at the apex of the tip. The process of light confinement can be considered as a superfocussing effect, because the intensity of the tightly confined light spot is significantly higher than that of the focussed yet much wider incident beam. The mechanism of superfocussing can be considered as a dimensional reduction of surface plasmon modes, where an edge plasmon is the most important link between the waveguide-modes inside the tip and the confined near field at the apex.

PACS 07.79.Fc · 78.67.-n · 42.82.Gw

K. Tanaka
Department of Electronics and Computer Engineering, Gifu University, Yanagido 1-1, Gifu 501-11, Japan
e-mail: tanaka@tnk.info.gifu-u.ac.jp

G.W. Burr
IBM Almaden Research Center, 650 Harry Road, San Jose, CA 95120, USA
e-mail: burr@almaden.ibm.com

T. Grosjean
Laboratoire d'Optique P. M. Duffieux UMR 6603, CNRS/Université de Franche-Comté, IMFC FR67 UFR Sciences et Technique, 25030 Bésaçon cedex, France
e-mail: thierry.grosjean@univ-fcomte.fr

T. Maletzky · U.C. Fischer (✉)
Physikalisches Institut, Westfälische Wilhelms-Universität Münster, Wilhelm-Klemm-Str. 10, 48149 Münster, Germany
e-mail: fischeu@uni-muenster.de

T. Maletzky
e-mail: maletzk@uni-muenster.de

1 Introduction

Metal-coated dielectric tetrahedral tips (T-tip) have long been considered to be interesting structures for the confinement of light to nanoscopic dimensions [1–4], and in particular as probes for scanning near-field optical microscopy (SNOM) [2, 3]. Metal-coated glass fragments of a tetrahedral shape have been used to image the photonic nanopatterns related to the surface plasmon excitation of metal nanostructures down to a resolution of 30 nm [5, 6]. Even higher resolution, on the order of 10 nm, was obtained in SNOM images of the granular structure of metal films [3, 7, 8] and of the domain structure of dye monolayers adsorbed to a metal substrate [9]. Recently a T-tip was also successfully used as a probe for tip-enhanced Raman spectroscopy [10, 11].

Metallic wedges have recently received attention as waveguiding structures [12–17], due to their tight modal

confinement and the prospect for device miniaturization beyond the optical wavelength limit. Metal-coated dielectric wedges are also an integral part of a metal-coated T-tip. Such wedges serve an important but not yet well-understood role within a T-tip, linking the incident beam within the dielectric tip to the strongly localized excitation at the sharp apex of the tip. There are a number of different surface plasmon modes that can be produced on a metal-coated dielectric wedge depending on the exact configuration of the metal coating. Slit or gap modes [12, 18] can exist if the metal film coating the tip is discontinuous across the edge separating two neighboring triangular faces. In the case of a continuous metal film, plasmon channel modes [13–15] can exist at the glass-metal interface of the metal-coated edge. And, as a third possibility, edge modes [16, 17] can be excited at the air-metal interface of a fully metal-coated edge.

Here we propose that the edge modes at the air-metal interface are responsible for the efficient confinement of a beam of light incident into a metal-coated T-tip polarized in the plane of incidence (the plane between the incident beam and one edge of the tip, referred to afterwards as the K1 edge). Pile et al. [16] calculated dispersion relations for edge modes on a solid metal wedge. These modes have a wavelength that is shorter than the wavelength of surface plasmon modes of a 2D metal surface, yet longer than the wavelength of a plane wave in glass of refractive index 1.5. Therefore it is conceivable that similar modes could exist on the edge of a metal-coated dielectric wedge. These modes could then be excited, in analogy to the conventional Kretschmann configuration for metal-dielectric thin-film stacks, by phase-matching a beam of light incident at an angle onto an edge in an Attenuated Total Reflection (ATR) configuration.

However, such an incident beam, polarized in the plane of incidence, interacts not only with the metal-coated edge but also with the neighboring metal-coated faces of the wedge (see Fig. 1). If this incident beam is oriented so as to phase-match the wavevector of the edge mode, the resulting incidence angle is then smaller than the angle that would lead to resonant excitation of the surface plasmon modes on the neighboring faces. However, damped 2D evanescent modes will still be excited on these faces, which can then converge towards the K1 edge and contribute to the excitation of the 1D edge mode. The resulting edge mode will travel along the K1 edge and lead to localized (0D) excitation at the apex of the tip. In this sense the confinement of the incident light to a highly localized excitation of the tip can be considered as a superfocussing of light by a dimensional reduction of surface plasmon modes, from damped 2-dimensional face modes to a 1D edge mode, to a particle-like 0-dimensional resonance. The particle can either be part of the metal-coated tip, a local gap-plasmon mode formed between the tip and a metal surface in close proximity, or a resonant dipolar structure such as a nearby dye molecule.

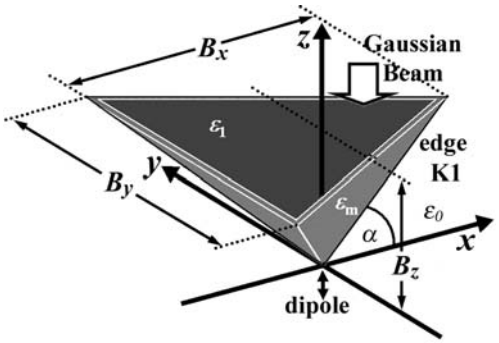

Fig. 1 Geometry of the T-tip. The body of the T-tip consists of glass of a dielectric constant $\varepsilon_1 = 2.25$. The glass structure is coated with a gold film of a thickness of 40 or 50 nm as specified in the text with a dielectric constant $\varepsilon_m = -3.515 - i2.9$ at 514 nm and $\varepsilon_m = -13.2 - i1.08$ at 633 nm, respectively. The angle between the x-axis and the K1 edge is $\alpha = 45°$, so that the angle between z-axis and K1 is also 45°. For FDTD calculations, the size of the tetrahedral tip is given by $B_x = 6.2$ µm, $B_y = 5.5$ µm, and $B_z = 3.1$ µm. A dipole source is placed at a distance of 10 nm below the tip. For VIE calculations, a Gaussian beam is incident along the z-axis into the tip with an extent defined by $B_x = 2276$ nm, $B_y = 2629$ nm, and $B_z = 1068$ nm. The tip-apex is placed at the origin of the coordinate-system

This concept of superfocussing is similar to those suggested by Bouhelier et al. [19] for the case of a tapered metal-coated cylindrical structure and by Keilmann [20] for a metal-coated curved circular structure. However, these structures do not have a metal covered edge as a link between 2D surface plasmon modes and the excitation at the apex of the tip. An alternate concept of superfocussing was suggested by Li et al. [21], who considered a superfocussing structure involving coupled resonances between nanoparticles of different sizes. However in our case, in addition to coupling between resonant structures, there is phase-matching between the incident beam, the damped surface plasmon modes, and the edge mode. We consider this sequential phase matching as an important property for efficient coupling between the incoming plane wave and the localized excitation.

Other superfocussing metal structures have been suggested as well, such as a metal cone [22, 23] and a metal-coated dielectric wedge [24–26]. These designs are based on a reduction of the wavelength of the surface plasmon modes with the taper of the structure. An incoming optical wavefront induces an end-fired excitation of surface plasmon modes at the wide end of the tapered structure. As surface plasmons travel along the tapered structure, the wavelength of the surface plasmon mode decreases continuously, leading to a highly localized excitation at the tip or small gap at the end of this structure. In comparison to the wedges within our T-tip, the metal-coated dielectric wedges discussed in [24–26] are nearly identical, except that the polarization of the incident beam is chosen to be perpendicular to the plane of incidence (the opposite of the T-tip case). The

superfocussing effect consists in the generation of a highly confined plasmon mode of an extremely small wavelength in a narrow gap between two metal faces. In our case, where no plasmon modes are excited with wavelengths that decrease with the progressive taper, the light confinement is generated at the metal-air interface. Finally, we mention that a complex structure for the confinement of a surface plasmon wave to edge modes on a solid metal wedge was proposed by Moreno et al. [17]. As before, the superfocussing effect is based on a gradual decrease of the wavelength of plasmon modes by an adiabatic introduction of the wedge shape.

Here we present detailed numerical investigations on the mechanism of how a beam of light incident into the metal-coated tetrahedral tip can generate a highly confined electric field at the apex of the tip. In Sect. 2, numerical investigations using the Finite-Difference Time-Domain (FDTD) method are used to explore the operation of the T-tip in extraction mode. A dipole source in close proximity to the apex of the tip excites the tip, revealing the field evolution in the tip, the resulting edge and face modes on the metal-coated surfaces, and the coupling from these modes into highly directional radiation into the dielectric interior of the tip. These results are the starting point for the illumination-mode numerical investigations of Sect. 3, where the volume integral method is used to compute the fields in the vicinity of the tip and in particular at the apex of the tip. These numerical calculations give a detailed account of how a highly confined excitation at the apex of the tip can be efficiently generated. In a following paper, the optical properties of a metal-coated tetrahedral tip will be compared to the numerical results.

2 Excitation of the T-tip in extraction mode by a dipole at the apex

The FDTD method [27] is a well-established method for rigorous simulation of Maxwell's Equations in nanophotonic and nanoplasmonic devices, including near-field optical tips [28, 29]. FDTD has the advantage of great flexibility in the structures and materials that can be simulated, at the expense of a Cartesian grid that can make it difficult to correctly model angled and curved surfaces. However, the advent of workstations with large amounts of memory and parallelized implementation on supercomputers such as BlueGene/L [30] has made it possible to simulate regions of many cubic wavelengths.

The model used for the calculations is shown in Fig. 1, consisting of a volume spanning ± 3.1 μm in x (with the K1 edge along $+x$) and ± 2.25 μm in y about the apex of a Tetrahedral-tip. The apex, with a tip-radius equal to the gold thickness of 50 nm, is located at $x = y = z = 0$. The simulation spans 0.75 μm below the tip in air and terminates 3.15 μm into the body of the tip. The gold layer is simulated using a simple Drude model to implement a dielectric constant of gold $\varepsilon_m = -3.515 - \mathrm{i}2.9$ at 514 nm and $\varepsilon_m = -13.2 - \mathrm{i}1.08$ at 633 nm, respectively [31]. The glass is considered to have a dielectric constant $\varepsilon_1 = 2.25$. The angle between the z-axis and the K1 edge (which projects down onto the $+x$-axis) and between the z-axis and the opposite face (which contains the projection onto the $-x$-axis) is 45°.

At $z = 3$ μm from the tip, the metal surfaces of the tip are terminated by a wide rectangular block of glass, preventing any surface plasmons from unphysically interacting with the Convolutional-PMLs [32] that terminate all six boundaries of the simulation volume. The nonuniform grid resolution varies from 25 nm for portions at the periphery of the simulation, to moderate resolution (10 nm in x, y and 5 nm in z) for regions closer than 1.5 μm in x, y, and $+z$ and closer than 200 nm in $-z$ below the apex. The region immediately around the apex (± 200 nm in x and y, ± 100 nm in z) is gridded at 2.5 nm. Unphysical reflections due to differences in numerical dispersion between these regions are suppressed [27]. The resulting simulations are roughly $550 \times 500 \times 475$ grid cells in size and require 50 minutes of simulation time to converge on a BlueGene/L partition with 512 dual-processor nodes.

To excite the T-tip in extraction mode, a single dipole oriented along a Cartesian direction is placed directly under the tip at a distance of 10 nm and excited with a simple monochromatic sinusoid. Figures 2a and 2b show the resulting E_x field distributions along $y = 0$ for dipoles oriented in the x-direction and excitation at a wavelength of 633 nm and 514 nm, respectively. There is a striking difference in the two figures. A noticeable evanescent field extends along the K1 edge ($+x$ side of the structure) at 633 nm (Fig. 2a), whereas this field is nearly absent at 514 nm (Fig. 2b).

In Fig. 2a, there are pronounced features in the field distribution along both the K1 edge and the opposite face ($-x$ side of the structure). Along the K1 edge, a clear edge plasmon mode is visible with a periodicity of 553 nm, smaller than both the vacuum wavelength of 633 nm and the 606 nm periodicity of the 2D surface plasmon mode at the metal-air interface of the opposing face. Furthermore, a beam of light is radiated into the tip starting from the K1 edge, clearly indicating a leaky edge mode. These edge plasmons lead to a strongly directional radiation of light into the glass tip at an angle of 40° with respect to the K1 edge. On the opposing face, evanescent fields extend along both the metal-glass and metal-air interfaces, with periodicities of 374 and 606 nm, respectively. 374 nm is the wavelength of a surface plasmon at the metal glass interface of a 50 nm thick gold film. There are also smaller periodicities of evanescent waves which cannot be identified with pure surface plasmon modes. These are most likely produced by beating between different modes. The beam radiated from the K1 edge can

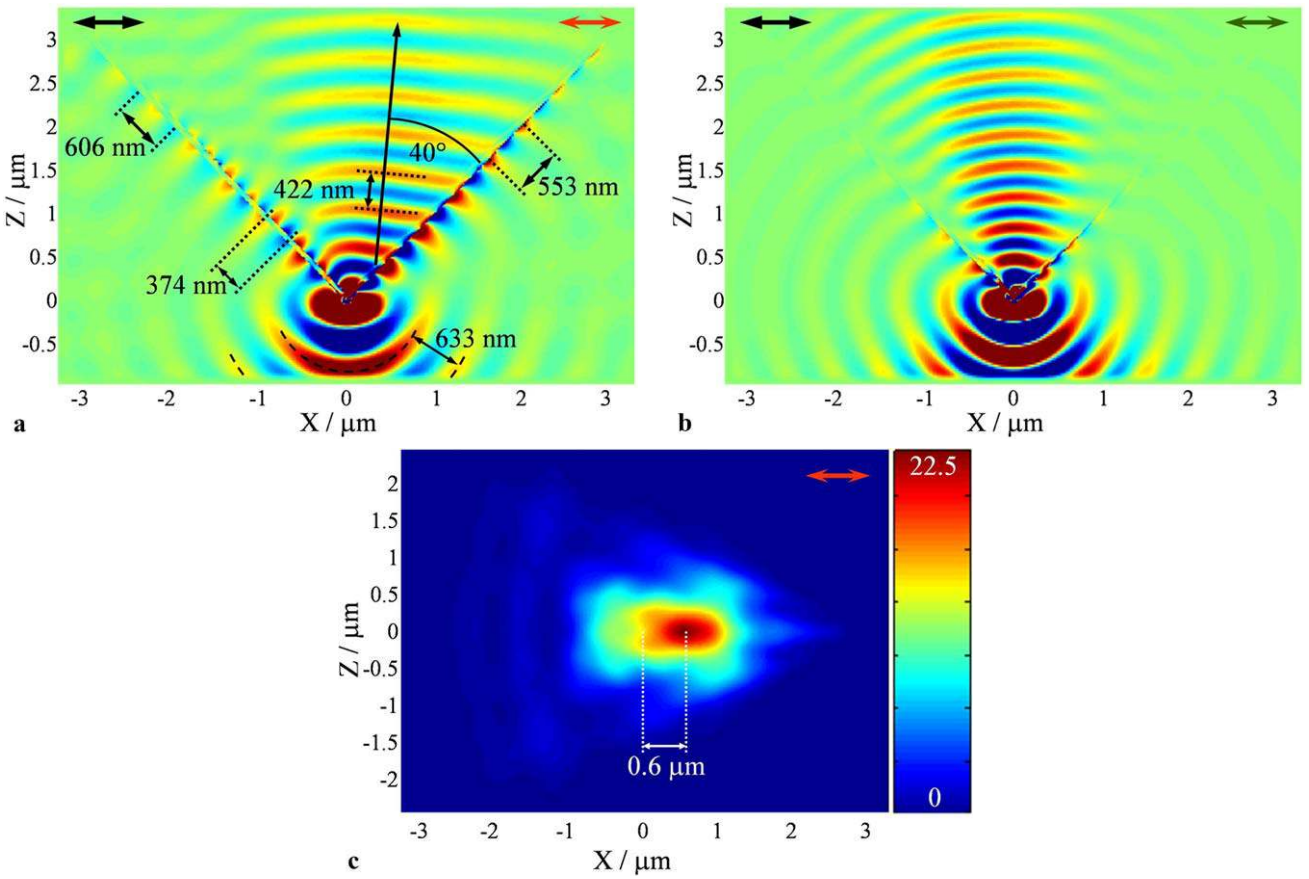

Fig. 2 Results of FDTD calculations excited by an x-oriented dipole at a distance of 10 nm from the tip. The *black arrow* indicates the direction of the electric field. (**a**) The x-component E_x of the electric field is shown for a cross-section through the tip in the xz-plane at $y = 0$. The vacuum wavelength is 633 nm. The *red arrow* indicates the orientation of the exciting dipole. (**b**) The same as (**a**) but the vacuum wavelength is 514 nm, and the *green arrow* indicates the orientation of the dipole. (**c**) Optical intensity ($|E_x|^2 + |E_y|^2 + |E_z|^2$) is shown for a cross-section through the tip in the xy-plane at $z = 3$ µm

also be observed in a z-slice 3.1 µm above the tip, as shown in Fig. 2c. At this plane, the combination of angled incidence and the distributed coupling along the K1 edge produces a directed beam that is displaced from the center of the tip by $x = 0.6$ µm as shown in Fig. 2c.

We also investigated the excitation of the tip produced by dipoles with different orientations. A z-polarized dipole at 633 nm excites several radiative bulk modes in the tip as shown in Fig. 3a. The edge mode of the K1 edge is strongly excited, and again the edge and 2D surface plasmon modes at the metal-air and the metal-glass interfaces can be identified. However, it is difficult to assign the origin of the radiative modes from the y-slice. A slice at $z = 3.1$ µm of Fig. 3b shows a nearly but not completely symmetric excitation of all three edges. This is not surprising because the z-direction does not coincide with the axis of symmetry of the tip (the angle of the K1 edge with respect to the $z = 0$ plane is identical to the face opposite, not to the other two edges). The angle between each edge and the axis of symmetry of the tip is 55°, but the angle between the K1 edge and the z-axis was chosen to be 45°, corresponding to the most typical experimental configuration [3].

3 Field confinement in the tetrahedral tip by a Gaussian beam incident into the tip

The results of Sect. 2 clearly show how the excitation of the T-tip by a dipole source leads to the excitation of leaky edge modes which are connected to a highly directional radiation into the dielectric interior of the tip at an angle of 40° with respect to the metal-coated edges. These results also give a hint of how to achieve a strongly localized excitation at the apex of the tip in illumination configuration where a focussed beam of light is incident into the tip. By using a volume integral equation method, the development of the field in and around the tip was calculated for a Gaussian beam incident into the tip at a direction of 45° with respect to the K1 edge of the tip.

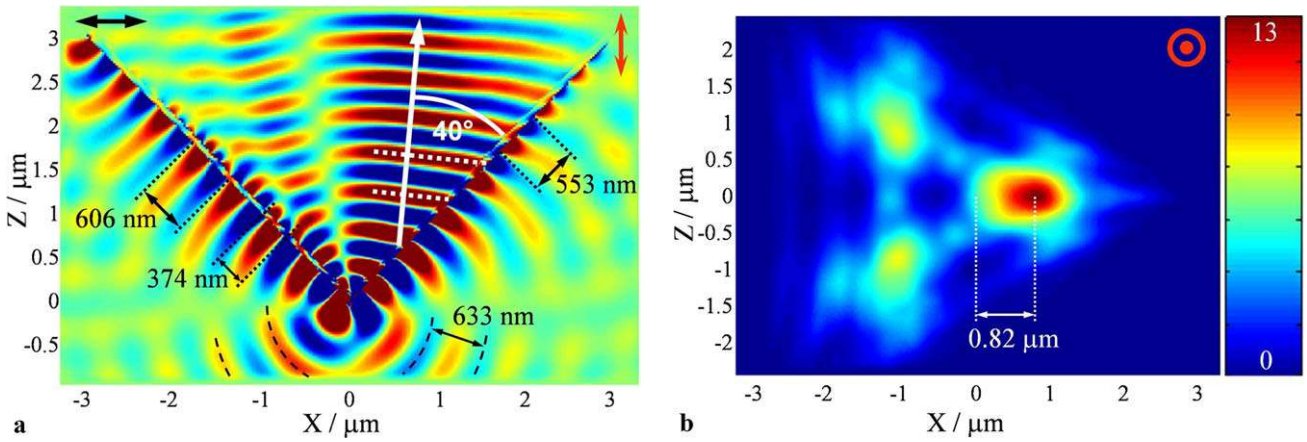

Fig. 3 Results of FDTD calculations excited by a z-oriented dipole at a distance of 10 nm from the tip. The x-component E_x of the electric field is shown. The direction of the electric field is indicated by *black arrows*, and the orientation of the dipole by *red symbols* (*arrow or target*). (**a**) The x-component E_x of the electric field is shown for a cross-section through the tip in the xz-plane at $y = 0$. The vacuum wavelength is 633 nm. (**b**) Optical intensity ($|E_x|^2 + |E_y|^2 + |E_z|^2$) is shown for a cross-section through the tip in the xy-plane at $z = 3$ µm

3.1 Numerical methods

The scattering problem for the metallic structure shown in Fig. 1 can be solved using a volume integral equation, under the assumption of harmonic $\exp(\mathrm{i}\omega t)$ time dependence [33], as

$$\mathbf{E}_i(\mathbf{x}) = \mathbf{D}(\mathbf{x})/\varepsilon_r(\mathbf{x}) - \big(k_0^2 + \nabla\nabla\cdot\big)\mathbf{A}(\mathbf{x}). \tag{1}$$

Here, $k_0 = \omega/\mathrm{c}$ (c is the velocity of light in free space, ω is the angular frequency), $\mathbf{D}(\mathbf{x})$ is the total electric flux, $\mathbf{E}_i(\mathbf{x})$ is the incident electric field, and $\mathbf{A}(\mathbf{x})$ is the vector potential, which is expressed by the following volume integral:

$$\mathbf{A}(\mathbf{x}) = \frac{1}{\varepsilon_0}\iiint_V \frac{\varepsilon_r(\mathbf{x}') - \varepsilon_0}{\varepsilon_r(\mathbf{x}')}\mathsf{G}(\mathbf{x},\mathbf{x}')\mathbf{D}(\mathbf{x}')\,\mathrm{d}^3x'. \tag{2}$$

Here, $\mathsf{G}(\mathbf{x},\mathbf{x}')$ is the three-dimensional free-space Green's function given by

$$\mathsf{G}(\mathbf{x},\mathbf{x}') = \frac{\mathrm{e}^{\mathrm{i}k_0|\mathbf{x}-\mathbf{x}'|}}{4\pi|\mathbf{x}-\mathbf{x}'|}. \tag{3}$$

The volume integral region V in (2) represents the entire space, and $\varepsilon_r(x)$ represents the distribution of permittivity, where $\varepsilon_r(x) = \varepsilon_m$ in the metallic coating, $\varepsilon_r(x) = \varepsilon_1$ in the dielectric region and $\varepsilon_r(x) = \varepsilon_0$ in free space. Since the region in which $|\varepsilon_r(x) - \varepsilon_0|$ is nonzero is finite and the integral region V has a finite volume, it is possible to solve (1) numerically by the well-established method of moments. To obtain the solution, the entire region of the problem is divided into small discretized cubes of size $\delta \times \delta \times \delta$, and (1) is discretized by the method of moments using roof-top functions as basis and testing functions. The resultant system of linear equations is then solved by iteration using a GMRES iteration with an FFT [33, 34].

The incident Gaussian beam, which propagates in the negative z-direction, can be expressed as follows [35]:

$$\begin{aligned}\mathbf{E}_i = {} & E_0\frac{W_0}{W(z)}\big[\mathbf{e}_x + \mathrm{i}\mathbf{e}_z\big(1+\gamma^2(z)\big)^{-1/2}\gamma(x)\mathrm{e}^{\mathrm{i}\Psi(z)}\big] \\ & \times \exp\left[-\frac{x^2+y^2}{W^2(z)}\right] \\ & \times \exp\left[-\mathrm{i}k_0\frac{(x^2+y^2)}{2R(z)}\right]\mathrm{e}^{\mathrm{i}\Psi(z)}\mathrm{e}^{+\mathrm{i}k_0 z},\end{aligned} \tag{4}$$

where

$$W(z) = W_0\big[1+\gamma^2(z)\big]^{1/2}, \qquad \Psi(z) = \arctan\gamma(z),$$

$$R(z) = -(z-z_0)\left[1+\frac{1}{\gamma^2(z)}\right], \qquad \gamma(z) = -2\frac{z-z_0}{k_0 W_0^2},$$

$$\gamma(x) = -\frac{2x}{k_0 W_0^2}.$$

E_0 is a constant amplitude-factor, W_0 is the radius of the spot size at $z = z_0$, and $\mathbf{e}_x$, $\mathbf{e}_z$ are the Cartesian unit-vectors. The validity of the code was checked by confirming that the code gives a reasonably accurate solution compared with the rigorous solution for a dielectric sphere and by confirming the energy conservation for a lossless problem under a paraxial approximation.

3.2 Results

The geometry of the model used for the calculations is shown in Fig. 1. The three surfaces of the glass structure are coated by a gold (Au) film of 40 nm thickness. The wavelength is 633 nm, and the relative permittivities of the glass and the gold are given by $\varepsilon_1/\varepsilon_0 = 2.25$ and

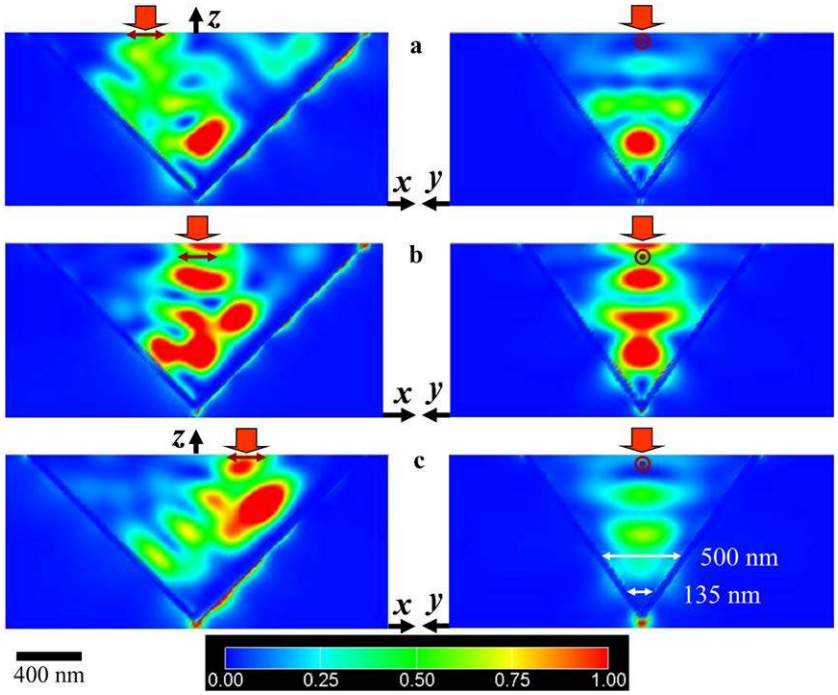

Fig. 4 The *left column* shows optical intensity distributions on the xz-plane $|E(x, 0, z)|^2$ and the *right column* shows those on the yz-plane $|\mathbf{E}(0, y, z)|^2$. The axis of the incident x-polarized beam is parallel to the z-axis and is centered at $y = 0$ and (**a**) $x = -302$ nm, (**b**) $x = 0$ nm, (**c**) $x = +302$ nm. Excitation vacuum-wavelength is $\lambda_0 = 633$ nm. The diameter of the Gaussian beam at $z = z_0 = 1068$ nm is $2W_0 = 0.8\lambda_0$. The intensity scale range is normalized by the incident intensity. In (**c**) the intensity saturates at the tip for a better visibility of the intensity distribution in the cross-section

$\varepsilon_m/\varepsilon_0 = -13.2 - \mathrm{i}1.08$, respectively. The Gaussian beam is incident perpendicularly to the xy-plane and at an angle of 45° with respect to both the K1 edge and the opposite face of the T-tip. The beam-waist is placed at $z = z_0 = 1068$ nm if not stated otherwise. The size of the Tetrahedral-tip is given by $B_x = 2276$ nm, $B_y = 2629$ nm, and $B_z = 1068$ nm and is discretized for the computation into cubes of size $\delta = 10$ nm.

Figure 4 shows the distribution of the optical intensity in cross-sections through the T-tip in the $(x, y = 0, z)$-plane and the $(x = 0, y, z)$-plane for different conditions. An intense and strongly confined spot at the apex of the tip is only obtained for a displacement of the incident beam away from the central z-axis of the T-tip by about $x = +302$ nm. In this case, there is an indication of a standing wave phenomenon along the K1 edge with an increasing intensity towards $z = 0$ nm. This standing wave can arise by the excitation of an edge mode which travels towards the tip and is partly reflected. For the other case, when the beam is displaced to $x = -302$ nm, a standing wave phenomenon also occurs. Here, however, the intensity of the standing wave is low at the tip apex and increases towards the edge of the simulation volume. This seems to be due to a wave travelling out of the tip which may be reflected at the rim of the tip, which in this model still has a rather limited size. From the data it is difficult to determine the period of the standing wave exactly. It seems, however, to be in the range of 270 and 280 nm, which is consistent with half the wavelength of the edge mode as determined in Sect. 2.

Figure 5 shows the intensity at a distance of 5 nm below the apex of the tip. This figure shows that there is a strongly confined spot of a high intensity when the incident beam is displaced in the x-direction to +302 nm from the center, and that this confined spot is absent when the beam is displaced to the other direction. The intensity is higher by a factor of 15 than the peak intensity in the focus of the incident Gaussian beam. The displacement is necessary to reach such a high intensity. This result shows that the edge plays an important role in the confinement of light to the apex of the tip.

It should be possible to further optimize the intensity at the apex of the tip by further adjustment of the experimental parameters. The results of Sect. 2 show that an angle of incidence of the Gaussian beam closer to 40° (instead of 45°) should lead to a more efficient excitation of the K1 edge mode. Furthermore, the optimal displacement of the beam from the center appears to be larger than 302 nm. We expect that a larger beam diameter would also lead to the accumulation of a higher field intensity. However, the limited size of the tip in these model calculations prevented us from fully optimizing the conditions for the confinement.

Figure 6 shows the optical intensity in the xy-plane at different z-values starting at 5 nm below the tip with z-increments of 101 nm. In Planes #1–4 of Fig. 6, one observes a redistribution of the intensity within the tip that is mainly due to reflections of the incident Gaussian beam at the faces of the tip. There are also evanescent fields outside of the tip which are distributed almost evenly at the faces and edges of the tip. From Plane #5 to Plane #8 it seems that the field is continuously expelled from the inside to the outside of the tip, and a strong evanescent field intensity gradually develops at the K1 edge and not at the faces of the tip.

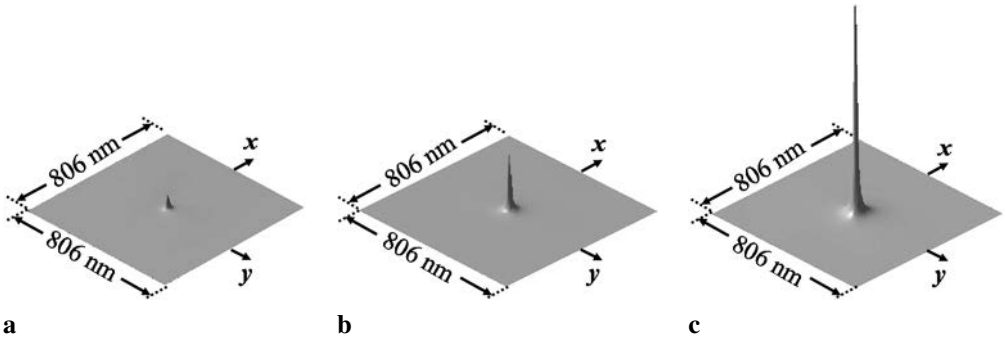

Fig. 5 Two-dimensional total optical intensity distributions just below the tip on a xy-plane placed at $z = -5$ nm, i.e., $|E(x, y, z = -5\text{ nm})|^2$ for beam parameters as in Fig. 4 and the x-position of the incident beam at (**a**) -302 nm, (**b**) 0 nm, and (**c**) $+302$ nm. The peak values of the intensities normalized by the incident intensity are about (**a**) 1.02, (**b**) 4.00, and (**c**) 15.1. The intensity scales are the same in all figures

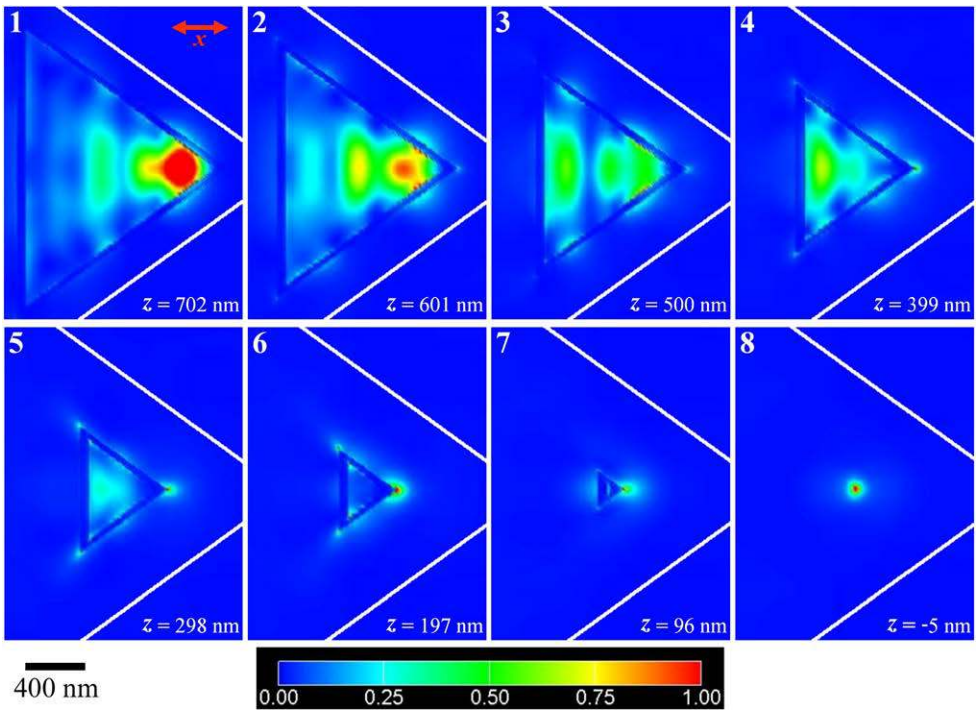

Fig. 6 Optical intensity distributions on xy-planes 1–8 for the same case as in Fig. 4c, where the beam axis is placed at $x = +302$ nm. Planes 1–8 are placed at equal intervals (101 nm) along the z-axis. The intensity is normalized to the incident beam. The *white lines* show the shape of the cross-section of the probe at $z = z_0 = 1068$ nm. The *red arrow* in the plane 1 indicates the incident x-polarization

The expulsion of the field from the inside of the tip is connected to a cut-off for the bulk modes at the inside of the metal-coated tip. Evanescent tails corresponding to damped surface plasmon modes excited by the bulk modes in glass at the faces of the tip disappear with a progression towards the apex. The edge mode however develops more and more, so that at the apex only a highly localized excitation remains.

3.3 Analogy to plasmon modes of a 1-D metal-insulator-metal sandwich

The rise of the edge mode at the expense of disappearing bulk and surface plasmon modes of the wedge structure is the essential ingredient for the superfocussing effect by a dimensional reduction of surface plasmon modes. In this process, the edge mode is excited by phase-matching from the beam incident at an oblique angle onto the edge. We can study this process of the excitation of an edge mode on a wedge-like structure in terms of surface plasmon modes of a sandwich system of two metal films separated by a dielectric slab [4], as indicated schematically in Fig. 7a. The modes of this metal–insulator–metal (MIM) sandwich structure as a function of the thickness d of the dielectric layer give an idea of the evolution of the mode structure in an adiabatically tapered wedge. While this analogy is useful for developing intuition about the complex properties of the strongly tapered 3-D tip, it is important to keep in mind that the simplicity of the 1-D MIM sandwich precludes it from being a completely realistic representation of the full 3-D apex of a T-tip.

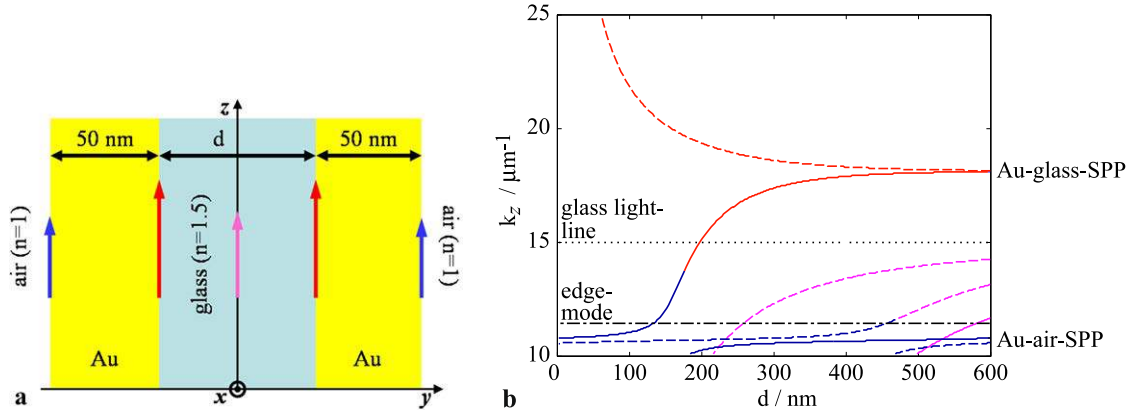

Fig. 7 1-dimensional metal–insulator–metal sandwich structure. (**a**) Scheme of the sandwich system. (**b**) Dispersion relations of the sandwich layer of 2 gold films of a thickness of 50 nm as a function of the thickness of the dielectric layer. Only *solid lines* correspond to antisymmetric modes. There is a transition of character of the surface plasmon modes where the electric field is concentrated at the metal air interface (*blue*) and at the metal glass interface (*red* respectively). For modes of a waveguide character, the field is concentrated in the dielectric (*purple*). The k-value of the edge plasmon mode $k_{\mathrm{edge}} = 11.35\ \mu\mathrm{m}^{-1}$ is indicated by the *black dash–dotted line*

As shown in Fig. 7b, the MIM sandwich system supports waveguide modes confined by the dielectric slab and surface plasmon modes at the metal-glass and the metal-air interfaces, respectively. Transverse magnetic modes of different symmetry exist which can be classified according to the symmetry of the magnetic field H_x. Only the antisymmetric modes are relevant for our wedge configuration because they match the symmetry of the polarization of the incident Gaussian beam (in the plane of incidence corresponding to the plane in the center of the sandwich structure). In the intensity distribution in the yz-plane of Fig. 4c, it is clear that the field intensity in the dielectric tip has a maximum and disappears gradually below a width of 500 nm as the tip gets narrower. This disappearance corresponds to a cut-off of the bulk waves in the dielectric. It can also be seen in this figure that evanescent tails of these bulk modes at the metal-air interface persist to a smaller width of about 135 nm. Decreasing the thickness further, the evanescent tails at the air interface also eventually disappear.

From the dispersion relations of the sandwich structure of Fig. 7b in this thickness range, the wavelength of the surface plasmon mode at the metal-glass interfaces increases strongly with decreasing thickness of the dielectric layer. In this range, a thickness is reached where these internal plasmon modes become phase-matched to the wavevector of the edge plasmon, so that the surface plasmons at the metal-glass interface can now be excited. Decreasing the width further, the phase matching condition is lost again. We conclude that there are, at different widths of the dielectric, different modes which have a phase-matching condition with the edge mode. These modes can couple to and excite the edge modes. This consideration shows how different channels contribute to the excitation of the edge mode.

The characteristic property—that the electric field intensity is expelled from the dielectric as the tip is approached and concentrates at the edge—can be attributed to the final channel. No strong electric field is developed by the antisymmetric plasmon modes in the dielectric because the polarization charges on the opposite faces have the same sign. Furthermore, for a very small thickness of the dielectric, the antisymmetric plasmon modes at the metal-glass interface change their field distribution so that the internal field is expelled to the outside. The plasmon modes at the metal-glass interfaces which are excited in the tapered gap of the wedge structure should be related to antisymmetric channel waveguide modes which were described by Novikov and Maradudin [13].

Figure 8 shows similar profiles as Fig. 4 for a wavelength of the incident light of 514 nm. Although a similar field distribution is observed as for 633 nm, the intensity of the electric field close to the apex of the tip is much lower in this case, and no pronounced standing wave phenomenon is observed at the edge. We attribute this difference to the strong damping of surface plasmon modes and edge modes for a gold coated tip at this wavelength as was shown in Sect. 2.

4 Discussion of the results of the numerical investigations

The numerical results reveal a mechanism of the confinement of light at the apex of a metal-coated dielectric tip of tetrahedral shape. We have shown that edge modes on the metal-coated wedge structures of the tip play an important role. The numerical results reveal that metal-coated edges

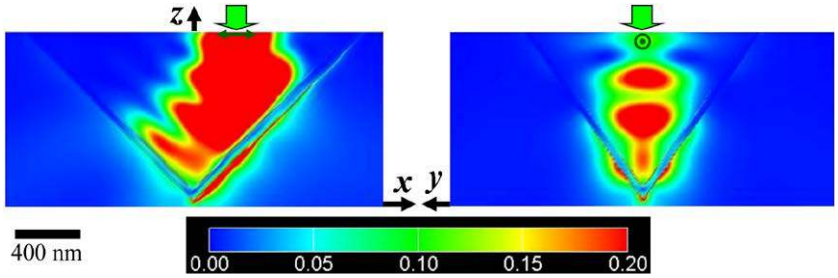

Fig. 8 For a vacuum-wavelength of $\lambda_0 = 514$ nm, the *left figure* shows the optical intensity distribution on the xz-plane $|\mathbf{E}(x,0,z)|^2$ and the *right figure* the one on the yz-plane $|\mathbf{E}(0,y,z)|^2$. The incident Gaussian beam is x-polarized and its axis is parallel to the z-axis and placed at $y = 0$, $x = +254$ nm. The diameter of the beam spot size at $z = 1068$ nm is $2W_0 = 0.8\lambda_0$. The intensity is normalized to the incident beam. Note that the scale ranges here from 0 to 0.2. The peak intensity at the position $z = -4$ nm corresponds to only 0.43 $\times$ the intensity of the incident beam

support leaky edge modes which are connected to highly directive radiative modes in the tip. The process of light confinement can be considered as a superfocussing effect because the intensity of the confined light spot is much higher than the one of the focussed incident beam and the confined spot is much smaller than the focus.

The mechanism of superfocussing can be considered as a dimensional reduction of surface plasmon modes. The numerical results reveal that as the incident beam propagates towards the apex of the tip, the electric field is expelled from the dielectric corner of the tip, first to the metal-air interface of the tip and then to an edge of the tip. An edge mode of increasing intensity delivers the energy to the apex of the tip. This process can be understood qualitatively by an interplay of an incident wave with the edge mode and surface plasmon modes on the metal-air and metal-dielectric interfaces. A beam of light is incident into the tip at an angle where it matches the phase of an edge mode. Thus it can directly excite the edge mode. But the incident beam also interacts with different surface plasmon modes of the metal-coated wedge structure of the tip. Where a phase matching condition is met, these modes can be excited by the incident beam, and the surface plasmon modes can in turn excite the edge mode. Thus different pathways exist for the excitation of the edge mode.

The numerical results give us a method for optimizing the parameters for tip excitation in terms of the composition of the tip, its geometry, and the configuration of the incident beam. These parameters can also be varied rather easily in our experimental configuration where the tip is realized by a glass fragment coated with metal [2, 3]. The type of glass and metal, the thickness of the metal coating as well as the form of the glass fragment can be varied over a wide range. In addition to the conventional coating of the glass fragment with a homogeneous metal film, the coating conditions can be varied so that different faces and edges of the fragment are coated with metal films of different thickness or metal composition. It is also possible to form tips where not all of the faces of the tip are coated or where not all of the edges are coated with metal, which introduces a slit in the metal coating exactly at the edge. Unlike in other configurations where tips are connected to fibres, the incident beam can be adjusted rather freely. It is possible to adjust the numerical aperture of the incident beam as well as its focus and polarization. We can also use radial polarization and structured illumination. This gives us a wide range for an experimental variation of the parameters. Thus the optimization of the tip can be performed by iterative experimental and numerical investigations.

The numerical calculations also show how a dipole source at the apex of the tip leads to a highly directional radiation into the body of the tip. They thus show how the radiation of a molecule into the T-tip can be used as a highly efficient pathway for signal detection in near-field optical microscopy and spectroscopy such as tip enhanced Raman Spectroscopy [10, 11]. The radiation into a narrow angular range facilitates the collection of the signal which would otherwise only be possible with optics of a high numerical aperture.

Edge modes are not only of interest in the context of the T-tip which we use as a probe for SNOM. Sharp metal edges are abundant in electronic semiconductor and other micro- and nanostructures. Thus they could be used to introduce additional nano-photonic functionalities in opto-electronic devices. The T-tip and related structures may well turn out to be well suited for quantum optics with surface plasmons [36, 37], as it contains the most important ingredients of such a structure, namely a strong field confinement and an efficient coupling to directed radiation. An important aspect in this context, especially for exploratory purposes to test functionality, is the simple fabrication scheme—just breaking a piece of glass and coating it with metal [2, 3]—as compared to elaborate nanofabrication techniques.

In terms of the numerical methods used here, we want to point out that the numerical FDTD method is not restricted to the case where a dipole excites the tip, nor is the VIE

method limited to the inverse case of a beam incident into the tip creating a local excitation at the apex. Both configurations can be treated with either method, and it will be possible to compare the result of the numerical methods and choose the most appropriate method for any particular problem.

Acknowledgement This work was partly supported in part by the German Research Foundation and the Network of Excellence Plasmo-Nano-Devices in the FP6 IST Program of the European Community.

References

1. T. Yatsui, M. Kourogi, M. Ohtsu, Plasmon waveguide for optical far/near-field conversion. Appl. Phys. Lett. **79**, 4583–4586 (2001)
2. U.C. Fischer, The tetrahedral tip as a probe for scanning near-field optical microscopy, in *Near-Field Optics*, ed. by D.W. Pohl, D. Courjon. NATO ASI Series E, vol. 242 (Kluwer Academic, Dordrecht, 1993), pp. 255–262
3. U.C. Fischer, J. Koglin, H. Fuchs, The tetrahedral tip as a probe for scanning near-field optical microscopy at 30 nm resolution. J. Microsc. **176**, 231–237 (1994)
4. U.C. Fischer, A. Dereux, J.-C. Weeber, Controlling light confinement by excitation of localized surface plasmons. Top. Appl. Phys. **81**, 49–69 (2001)
5. H.-J. Maas, A. Naber, H. Fuchs, U.C. Fischer, J.C. Weeber, A. Dereux, Imaging of photonic nanopatterns by scanning near-field optical microscopy. Opt. Soc. Am. B **19**, 1295–1300 (2002)
6. H.-J. Maas, J. Heimel, H. Fuchs, U.C. Fischer, J.C. Weeber, A. Dereux, Photonic nanopatterns of gold nanostructures indicate the excitation of surface plasmon modes of a wavelength of 50–100 nm by scanning near-field optical microscopy. J. Microsc. **209**, 241–248 (2003)
7. J. Heimel, U.C. Fischer, H. Fuchs, SNOM/STM using a tetrahedral tip and a sensitive current-to-voltage converter. J. Microsc. **202**, 53–59 (2001)
8. U.C. Fischer, J. Heimel, H.-J. Maas, H. Fuchs, J.C. Weeber, A. Dereux, Super-resolution scanning near-field optical microscopy, in *Optical Nanotechnologies—the Manipulation of Surface and Local Plasmons*, ed. by J. Tominaga, D.P. Tsai. Topics in Applied Physics, vol. 88 (Springer, Berlin, 2003), pp. 141–151
9. E.G. Bortchagovsky, J. Heimel, H. Fuchs, U.C. Fischer, Dual wavelength snom imaging of monolayers of j-aggregated dye molecules. J. Korean Phys. Soc. **47**, S48–S55 (2005)
10. S. Klein, J. Reichert, H. Fuchs, U.C. Fischer, Near-field Raman spectroscopy using a tetrahedral snom tip, in *Proc. of SPIE*, vol. 6195 61951F (1–7), 2006
11. E.G. Bortchagovsky, S. Klein, H. Fuchs, U.C. Fischer, Surface plasmon mediated tip enhanced Raman scattering. Oral contribution to the XXI International Conference on Raman Spectroscopy ICORS, 17–22 August 2008. Uxbridge, West London, UK
12. G. Veronis, S. Fan, Guided subwavelength plasmonic mode supported by a slot in a thin metal film. Opt. Lett. **30**, 3359–3361 (2005)
13. I.V. Novikov, A.A. Maradudin, Channel polaritons. Phys. Rev. B **66**, 035403 (2002)
14. D.K. Gramotnev, D.F.P. Pile, Single mode subwavelength waveguide with channel plasmon-polaritons in triangular grooves on a metal surface. Appl. Phys. Lett. **86**, 6323–6325 (2006)
15. S. Bozhevolnyi, V.S. Volkov, E. Devaux, J.-Y. Laluet, T.W. Ebbesen, Channel plasmon subwavelength waveguide components including interferometers and ring resonators. Nature **440**, 508–510 (2006)
16. D.F.P. Pile, T. Oawa, D.K. Gamotnev, T. Okamoto, M. Haraguchi, M. Fukui, S. Matsuo, Theoretical and experimental investigation of strongly localized plasmons on triangular metal wedges for subwavelength waveguiding. Appl. Phys. Lett. **87**, 061106 (2005)
17. E. Moreno, S.G. Rodrigo, S.I. Bozhevolnyi, L. Martin Moreno, F.J. Garcia-Vidal, Guiding and focusing of electromagnetic fields with wedge plasmon polaritons. Phys. Rev. Lett. **100**, 023901 (2008)
18. K. Tanaka, M. Tanaka, Simulations of nanometric optical circuits based on surface plasmon polariton gap waveguide. Appl. Phys. Lett. **82**(8) (2003)
19. A. Bouhelier, J. Renger, M.R. Beversluis, L. Novotny, Plasmon—coupled tip enhanced near-field microscopy. J. Microsc. **210**, 220–224 (2002)
20. F. Keilmann, Surface polariton propagation for scanning near-field microscopy. J. Microsc. **194**, 567 (1999)
21. K. Li, M.I. Stockman, D.J. Bergman, Self similar chain of metal nanospheres as an efficient nanolens. Phys. Rev. Lett. **91**, 2274021 (2003)
22. A.J. Babadjanyan, N.L. Margaryan, Kh.V. Nerkararyan, Superfocusing of surface polaritons in the conical structure. J. Appl. Phys. **87**(8), 3785–3788 (2000)
23. M.I. Stockman, Nanofocussing of optical energy in tapered plasmonic waveguides. Phys. Rev Lett. **93**, 137404 (2004)
24. Kh.V. Nerkarayan, Superfocussing of a surface polariton in a wedge-like structure. Phys. Lett. A **237**, 103–105 (1997)
25. D.F.P. Pile, D.K. Gramotnev, Adiabatic and non adiabatic nanofocusing of plasmons by tapered gap plasmon waveguides. Appl. Phys. Lett. **89**, 041111 (2006)
26. D.K. Gramotnev, Adiabatic nanofocussing of plasmons by sharp metallic grooves: Geometrical optics approach. J. Appl. Phys. **98**, 104302 (2005)
27. A. Taflove, S.C. Hagness, *Computational Electrodynamics: The Finite-Difference Time-Domain Method*, 3rd edn. (Artech House, Boston, 2005)
28. D.A. Christensen, Analysis of near-field tip patterns including object interaction using finite-difference time-domain calculations. Ultramicroscopy **57**(2–3), 189–195 (1995)
29. J.L. Kann, T.D. Milster, F.F. Froehlich, R.W. Ziolkowski, J.B. Judkins, Linear behavior of a near-field optical-scanning system. J. Opt. Soc. Am. A **12**(8), 1677–1682 (1995)
30. A. Gara, M.A. Blumrich, D. Chen, G.L.T. Chiu, P. Coteus, M.E. Giampapa, R.A. Haring, P. Heidelberger, D. Hoenicke, G.V. Kopcsay, T.A. Liebsch, M. Ohmacht, B.D. Steinmacher-Burow, T. Takken, P. Vranas, Overview of the Blue Gene/L system architecture. IBM J. Res. Dev. **49**(2–3), 195–212 (2005)
31. P.B. Johnson, R.W. Christy, Optical constants of the noble metals. Phys. Rev. B **6**(12), 4370–4379 (1972)
32. J.A. Roden, S.D. Gedney, Convolution PML (CPML): an efficient fdtd implementation of the CFS-PML for arbitrary media. Microw. Opt. Technol. Lett. **27**(5), 334–339 (2000)
33. P. Zwamborn, P.M. van den Berg, The three-dimensional weak form of the conjugate gradient FFT method for solving scattering problems. IEEE Trans. MTT **40**, 1757–1766 (1992)
34. K. Tanaka, M. Tanaka, T. Sugiyama, Simulation of practical nanometric optical circuits based on surface plasmon polariton gap waveguide. Opt. Express **13**(1), 256–266 (2005)
35. G.S. Smith, *An Introduction to Classical Electromagnetic Radiation* (Cambridge University Press, Cambridge, 1997)
36. D.E. Chang, A.S. Soerensen, P.R. Hemmer, M.D. Lukin, Quantum optics with surface plasmons. Phys. Rev. Lett. **97**, 053002 (2006)
37. D.E. Chang, A.S. Soerensen, P.R. Hemmer, M.D. Lukin, Strong coupling of single emitters to surface plasmons. Phys. Rev. B **76**, 035402 (2007)